Iris Recognition with Adaptive Coding

Adam Czajka and Andrzej Pacut

Institute of Control and Computation Engineering
Warsaw University of Technology
Nowowiejska 15/19, 00-665 Warsaw, Poland
Biometric Laboratories
Research and Academic Computer Network NASK
Wawozowa 18, 02-796 Warsaw, Poland
{A.Czajka,A.Pacut}@ia.pw.edu.pl, www.BiometricLabs.pl

Abstract. The paper proposes a new iris coding method based on Zak-Gabor wavelet packets. Details of the Zak-Gabor-based coding are presented in the paper, and the method of adaptation the transformation parameters is described. The methodology may be of particular help in development mobile iris systems, where the iris capture devices may present a limited quality. The method was evaluated and presents very favorable results.

Keywords: Iris recognition, biometrics.

1 Iris Measurement and Preprocessing

Biometric authentication starts from acquisition of appropriate biological data characteristic of an individual. We use a dedicated hardware designed and constructed to capture the iris from a convenient distance, with the desired speed and a minimal user cooperation. To illuminate iris we apply a near infrared 850 nm light that meets the ISO recommendations [1]. The system uses the pupil position estimated in real time to guide a person to position the eye, and to release the image capturing process. In this process several frames are captured at varying focal lengths, and the sharpest frame is selected for further analysis. The latter procedure compensates a small depths-of-field typical in iris imaging.

The raw images contain the iris and its surroundings. The iris must be first localized. To detect a boundary between the pupil and the iris, we propose a method which is sensitive to circular dark shapes, and unresponsive to other dark areas as well as light circles, such as specular reflections. This may be achieved by a modified Hough transform that uses the *directional image* to employ the image gradient, rather than the *edge image*, which neglects the gradient direction. A boundary between the iris and the sclera may be approximated by a circle. To determine this boundary, we independently apply Daugman's integro-differential operator [2] to two opposite horizontally placed angular sectors, 45° each, since the entire circular iris boundary may be partially disturbed by eyelids. The two radii of the resulting arcs are averaged to construct a circle approximating the outer iris boundary.

J.T. Yao et al. (Eds.): RSKT 2007, LNAI 4481, pp. 195–202, 2007.

The iris ring limited by the two circular boundaries may still be disrupted by irregular objects like reflections or eyelashes. It is desirable to use occlusion detection that does not assume any particular occlusion shape. We localize non-uniformity points within the iris ring and then construct an occlusion map. First, we calculate the sample variances of the iris image intensity for a set of radial sectors. These variances are compared to the maximum allowed variance obtained for directions in which the probability of iris occlusion is minimal. Those directions in which the calculated variance exceeds the threshold value is marked as an occlusion direction, and the appropriate occlusion radius is stored.

Based on the localized occlusions, we select two opposite 90° wide angular iris sectors. Each iris sector is then transformed by resampling and smoothing to a $P \times R$ rectangle, where $P = 512$ and $R = 16$. The rows f_ℓ of these two rectangles will be further referred to as the *iris stripes*. The experiments (see also [2]) revealed much higher correlation of the iris image in the radial direction, i.e. along the iris stripes, as compared to the angular direction, across the stripes. Figure 1 illustrates the preprocessed iris image and the corresponding iris stripes.

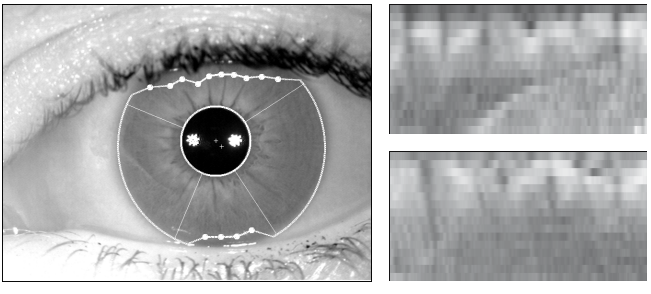

Fig. 1. *Left:* raw camera image processed by our system. The eyelids were automatically detected, and the sectors free of occlusions (marked as white full circles) are selected. Star-like shapes on the pupil are reflections of the illumination NIR diodes, and the '+' marks represent the pupil and the iris centers. *Right:* iris stripes automatically determined for the image shown on the left.

2 Database of Iris Images

Calculations in this work are employing our proprietary database of 720 iris images. The data was collected for 180 different eyes, with 4 images of each eye. We used 3 images of each eye in the estimation stage to calculate the iris templates, and the remaining single image of each eye in the verification stage. Typically, in iris capturing systems with one-eye capture optics, the images taken may be mutually rotated. Thus the mutual rotation of images used in the estimation stage was corrected using the correlation between images. The remaining fourth image was not altered.

3 Iris Features

3.1 Choice of Features

It is often convenient to characterize a discrete-time signal in the frequency domain, thus describing stationary energy distribution. For non-stationary signals, it might be worthwhile to characterize the frequencies locally, and to find the distribution of signal energy in local (possibly overlapping) time segments by application of *time-frequency* or *time-scale* analysis. Similarly, any constant (time-independent) space-homogeneous 1D or 2D pattern can be characterized in a 1D or 2D frequency domain. If a pattern is not space-homogeneous, its spatial frequency contents may be analyzed locally, with the use of *space-frequency* or *space-scale analysis*. Although the iris texture makes a 2D pattern, we simplify it to a set of 1D patterns with a certain loss of information and apply the space-frequency analysis locally to the iris circular sectors to describe their local features and to construct a compact iris features set.

There exist various tools to represent the signal in the mixed space-frequency domain. A family of Windowed Fourier Transforms apply Fourier Transform to windowed signals in time or space. The Gabor transform belongs to this family, and uses a Gaussian window characterized by its width. The window width significantly influences the resulting iris features and must be carefully chosen. We use the space-frequency analysis that employs waveforms indexed by space, scale and frequency simultaneously, what results in a larger set of possible tilling in the space-frequency plane, possibly redundant. This directs our methodology toward a *wavelet packet* analysis. There is a need to select appropriate frequencies and scales simultaneously to make the transformation sensitive to individual features existing in the iris image. In this paper we propose a systematic selection of appropriate scales and frequencies of the iris coding. This approach enables our method to be applied for databases of images of various resolution.

3.2 Application of Zak's Transform

Gaussian-shaped windows are not orthogonal, i.e., the inner product of any two windows is nonzero, therefore Gabor's expansion coefficients cannot be determined in a simple way. The fastest method of Gabor's expansion coefficients determination consists of application of Zak's transform [3] and is often referred to as Zak-Gabor's transform. We outline briefly Zak-Gabor's transform for a single iris stripe and a fixed window width.

Denote by g_s a one-dimensional Gaussian elementary function of the width index s, sampled at points $0, \ldots, P-1$, namely

$$g_s(p) = e^{-\pi\left((p+\frac{1}{2})/2^s\right)^2}, \quad p = 0, \ldots, P-1 \tag{1}$$

where $s = 2, \ldots, S$, and for the stripe length $P = 512$ we set $S = 8$. If P is (typically) chosen to be even, the $\frac{1}{2}$ term in (1) makes g_s to be an even function.

Let M be the number of possible translations of g_s, and K be the number of frequency shifts, where, following Bastiaans [3], we always take $M = P/K$. A shifted and modulated version $g_{mk;s}$ of the elementary function g_s can be constructed, namely

$$g_{mk;s}(p) = g_s(p - mK)e^{ikp2\pi/K}, \quad p = 0 \dots P-1 \tag{2}$$

where $m = 0, \dots, M-1$ and $k = 0, \dots, K-1$ denote the space and frequency shifts, respectively, and g_s is wrapped around in the P-point domain. The finite discrete Gabor transform of the iris stripe f_ℓ is defined as a set of complex coefficients $a_{mk;s\ell}$ that satisfy the Gabor signal expansion relationship, namely

$$f_\ell(p) = \sum_{m=0}^{M-1} \sum_{k=0}^{K-1} a_{mk;s\ell} g_{mk;s}(p), \quad p = 0 \dots P-1 \tag{3}$$

Following Bastiaans [3], we further set $K = 2^s$. Note that once the frequency index k is kept constant, $g_{mk;s}$ may be localized in frequency by a modification of s. This is done identically as the scaling in a wavelet analysis, hence we call s the *scale* index. The number of Gabor expansion coefficients $a_{mk;s\ell}$ may be interpreted as the signal's number of degrees of freedom. Note that the number S of scales together with the stripe size P determine both M and K.

The discrete finite Zak transform $\mathscr{Z} f_\ell(\rho, \phi; K, M)$ of a signal f_ℓ sampled equidistantly at P points is defined as the one-dimensional discrete Fourier transform of the sequence $f_\ell(\rho + jK)$, $j = 0, \dots, M-1$, namely [3]

$$\mathscr{Z} f_\ell(\rho, \phi; K, M) = \sum_{j=0}^{M-1} f_\ell(\rho + jK) e^{-ij\phi 2\pi/M} \tag{4}$$

where $M = P/K$. Discrete Zak's transform is periodic both in frequency ϕ (with the period $2\pi/M$) and location ρ (with the period K). We choose ϕ and ρ within the fundamental Zak interval [3], namely $\phi = 0, 1, \dots, M-1$ and $\rho = 0, 1, \dots, K-1$.

Application of the discrete Zak transform to both sides of (3) and rearranging the factors yields

$$\begin{aligned}
\mathscr{Z} f_\ell(\rho, \phi; K, M) &= \sum_{j}^{M-1} \left[\sum_{m}^{M-1} \sum_{k}^{K-1} a_{mk;s\ell} g_s(\rho + jK - mK) e^{ik\rho 2\pi/K} \right] e^{-ij\phi 2\pi/M} \\
&= \left[\sum_{m=0}^{M-1} \sum_{k=0}^{K-1} a_{mk;s\ell} e^{-i2\pi(m\phi/M - k\rho/K)} \right] \left[\sum_{j=0}^{M-1} g_s\big(\rho + jK\big) e^{-i2\pi j\phi/M} \right] \\
&= \mathscr{F} a_{s\ell}(\rho, \phi; K, M)\, \mathscr{Z} g_s(\rho, \phi; K, M)
\end{aligned} \tag{5}$$

where $\mathscr{F} a_{s\ell}[\rho, \phi; K, M]$ denotes the discrete 2D Fourier transform of an array of $a_{s\ell}$ that represents Gabor's expansion coefficients determined for the iris stripe

f_ℓ and scale s, and $\mathscr{Z}g_s[\rho,\phi;K,M]$ is discrete Zak's transform of the elementary function g_s. This shows that Gabor's expansion coefficients can be recovered from the product form (5). Once K and M are chosen to be powers of 2 (making also the signal length P to be a power of 2), the calculation of both $\mathscr{Z}f[\rho,\phi;K,M]$ and $\mathscr{Z}g[\rho,\phi;K,M]$, and inversion of 2D Fourier series can employ Fast Fourier Transform thus yielding computation times proportional to those in the FFT.

3.3 Definition of Iris Features

Calculation of Gabor's transform for all iris stripes and for all scales results in a set of coefficients a indexed by the quadruple: within-stripe position, frequency index, scale and stripe index (m,k,s,ℓ). Inspired by Daugman's work [2], we define the signs of the real and imaginary parts of Zak-Gabor coefficients as the feature set $\mathbb{B}$, namely

$$\mathbb{B} = \{\mathrm{sgn}(\Re(a_{mk;s\ell})),\ \mathrm{sgn}(\Im(a_{mk;s\ell}))\} \tag{6}$$

where $m = 0,\ldots,M-1$, $k = 0,\ldots,K-1$, $\ell = 0,\ldots,2R-1$ and $s = 2,\ldots,S$. Since Fourier's transform is symmetrical for real signals, for each position m the coefficients with the frequency index $k > K/2$ can be ignored. Since $M = P/K$, for each s there are $(N-1)P/2$ coefficients to be determined. Taking into account that this analysis is carried out for all iris stripes, and remembering that $R = 16, S = 8$ and $P = 512$, the total number of coefficients calculated for the iris image is $R(S-1)P = 57,344$. Both real and imaginary parts are coded separately by one bit, hence $N = |\mathbb{B}| = 114,688$ features may be achieved, where $|\cdot|$ denotes the number of elements in a finite set. The features, positioned identically for each iris, may thus form a binary vector. Thus, matching two features requires only a single XOR operation, and the Hamming distance can be applied to calculate the score.

We stress that $\mathbb{B}$ should not be confused with the so called *iriscode*™ invented by Daugman. The latter one is a result of an iris image filtering, while $\mathbb{B}$ is constructed with Gabor expansion coefficients.

3.4 Features Selection

The feature set $\mathbb{B}$ selected so far is oversized and only its certain subset will be included into the final feature set. All elements of $\mathbb{B}$ will thus be considered the *candidate features*. We propose a two-stage method that selects Zak-Gabor coefficients. We further consider partitions of all candidate features $\mathbb{B}$ onto *candidate feature families* $\mathbb{B}_{k,s}$, which represent all candidate features that are labeled by the same scale k and frequency s, and differ by space indices m and ℓ, namely

$$\mathbb{B}_{k,s} = \{\mathrm{sgn}(\Re(a_{mk;s\ell})), \mathrm{sgn}(\Im(a_{mk;s\ell})) : m = 0,\ldots,M-1, \ell = 0,\ldots,2R-1\}$$

Stage one: selection of useful features. The first selection stage consists of choosing a subset $\mathbb{B}^0$ of candidate features $\mathbb{B}$, called here the *useful features*. To determine $\mathbb{B}^0$, we analyze a variability of candidate features. For each feature b

we calculate the *within-eye sum of squares* $SS^W(b)$, and the *between-eye sum of squares* $SS^B(b)$. We categorize the features to maximize SS^B and minimize SS^W. We tried several methods to solve this multicriteria maximization problem. The best results were obtained when we minimized the distance from the most desired point on $SS^W \times SS^B$ plane. This point was set as $\big(\min_{b\in\mathbb{B}} SS^W(b), \max_{b\in\mathbb{B}} SS^B(b)\big)$, Fig. 2 (left).

We use the order introduced by the above procedure in the set of candidate features $\mathbb{B}$ in a procedure removing a high correlation of candidate features to increase an 'information density'. We include k-th candidate feature into the set $\mathbb{B}^0$ only if it is *not strongly correlated* with all the features already selected.

We base our useful feature definition on the *decidability coefficient* d' [2] calculated for a given feature subset. We calculate the decidability coefficient for each set of candidate features included into $\mathbb{B}^0$. The decidability varies with the number of candidate features included: it first grows to reach the maximum and then decreases. Experiments show that the decidability d' is highest for the correlation threshold around 0.3, Fig. 2 (right). For this solution there is no between-eye – within-eye overlap of sample distributions, i.e., there are no false matches and no false non-match examples in the estimation data set. The resulting 324 useful features pass to the second feature selection stage. We may add that our procedure included only such features for which $SS^W < SS^B$.

The higher is the number $\nu(k,s)$ of useful features in the candidate features family $\mathbb{B}_{k,s}$, the more important is (k,s) in iris recognition. This enables to categorize these families in the next stage of our selection procedure.

Stage two: selection of feature families $\mathbb{B}_{k,s}$. To finally decide for the best frequencies k and scales s, independently for real or imaginary parts of the Zak-Gabor coefficients, we sort $\mathbb{B}_{k,s}$ by decreasing $\nu(k,s)$ separately for real and imaginary parts of coefficients. This procedure prioritizes the families that are

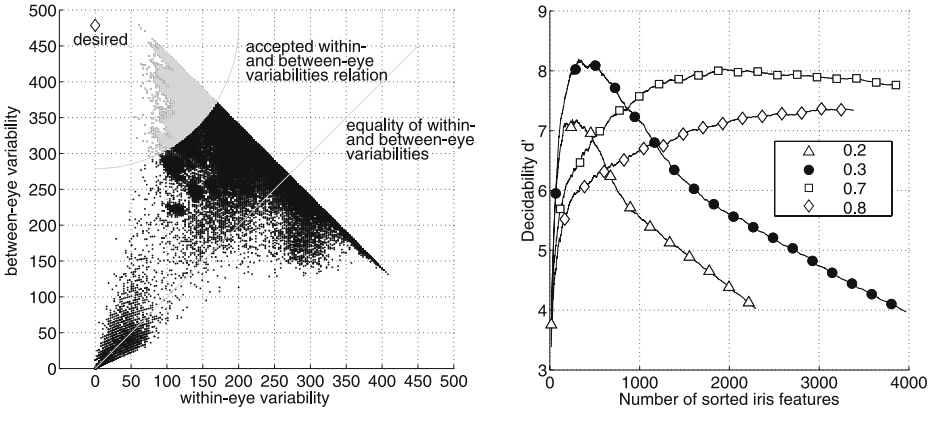

Fig. 2. *Left:* within-eye sum of squares vs. between-eye sum of squares and the area of *useful features. Right:* the decidability coefficient vs. number of useful features selected for a few correlation thresholds allowed within the useful features set.

most frequently 'populated' by the useful features. Such candidate feature families resulting in maximum d' are selected to the *final feature set*. This finally produces the iris feature set of 1024 bits (128 bytes), containing only four families. For this final feature set, we achieved the maximum decidability d' and no sample verification errors.

3.5 Features Personalization

Once the optimal feature families, namely the best scale-frequency pairs indexed by s and k, are selected, the iris features set is calculated for those chosen s and k and all $m = 1, \ldots, M-1$, and $\ell = 0, \ldots, 2R-1$. Each Zak-Gabor coefficient can 'measure' the correlation between the modulated Gaussian elementary function $g_{mk;s}$ and the corresponding stripe. The question arises how 'robust' are the consecutive Zak-Gabor coefficients against noise, and iris tissue elastic constrictions and dilations.

Due to a significant variability of the iris tissue, some $g_{mk;s}$ may not conform with the iris body, resulting in small coefficients. Such a situation is dangerous, since once the coefficients are close to zero, their signs may depend mostly on a camera noise, and consequently may weaken the final code. This motivates personalization of the iris feature sets that employ only those Zak-Gabor coefficients that exceed experimentally determined threshold, for which the decidability was maximal. Experiments show a far better discrimination between the irises if the personalized coding is employed.

3.6 Template Creation and Verification

Typically, more than one iris image is available for enrollment. For a given eye, a distance is calculated between a feature set of each image and the feature sets calculated for the remaining enrollment images. As the iris template we select this feature set, for which this distance is minimal.

Small eyeball rotations in consecutive images may lead to considerable deterioration of within-eye comparison scores. This rotation can be corrected by maximizing the correlation within the images enrolled. Since during verification the iris image corresponding to the template is unavailable, another methodology must be applied. We use an iterative minimization of the comparison score between Zak-Gabor-based features determined for a set of small artificial shifts of the iris stripes being verified.

4 System Evaluation and Summary

Figure 3 shows a sample distributions of genuine and impostor comparison scores achieved for the proposed coding. No sample errors were observed (FRR=FAR=0%) for the database used. However, the results must be taken with care since we used various images of the same eyes for estimation as well as for verification. Considering statistical guarantees and assuming 95% confidence level for the results obtained we expect FRR < 0.017 and FAR $\in \langle 0.000093, 0.03 \rangle$ in this approach.

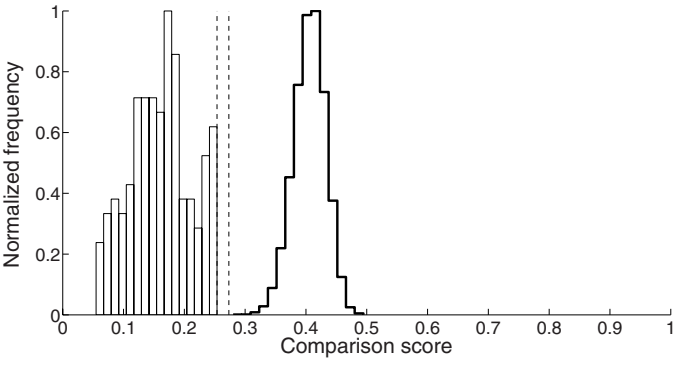

Fig. 3. Sample distributions of genuine and impostor comparison scores in the verification stage achieved for Zak-Gabor-based personalized coding with iterative eye rotation correction. No sample errors were encountered.

The Zak-Gabor coding was used in a number of applications, for instance in remote access scenario [4], in BioSec European project for the purpose of the biometric smart card development and it is also an element of the original iris recognition system prototype with eye aliveness detection [5]. Our feature selection procedure can be applied also to other iris coding methods.

References

1. American National Standards Institute: Information technology — Biometric data interchange formats — Part 6: Iris image data. ISO/IEC 19794-6:2005. ANSI (2005)
2. Daugman, J.: How iris recognition works. IEEE Transactions on circuits and systems for video technology **14** (2004)
3. Bastiaans, M.J.: Gabor's expansion and the zak transform for continuous-time and discrete-time signals. In Zeevi, J., Coifman, R., eds.: Signal and Image Representation in Combined Spaces. Academic Press, Inc. (1995) 1–43
4. Pacut, A., Czajka, A., Strzelczyk, P.: Iris biometrics for secure remote access. In Kowalik, J., ed.: Cyberspace Security and Defense: Research Issues. Springer (2005) 259–278
5. Pacut, A., Czajka, A.: Aliveness detection for iris biometrics. In: 2006 IEEE International Carnahan Conference on Security Technology, 40th Annual Conference, October 17-19, Lexington, Kentucky, USA, IEEE (2006) 122–129